*Desalination and Water Treatment*
www.deswater.com

doi: 10.5004/dwt.2023.29355

287 (2023) 67–79
March

# Electrochemical purification of Disperse Red 167 azo dye-based synthetic wastewater through the electrooxidation and electrocoagulation with Fe ions derived from Cu/Fe macro-corrosion galvanic cell

Mateusz Łuba[a,b], Tomasz Mikołajczyk[a,*], Mateusz Kuczyński[a], Bogusław Pierożyński[a], Agnieszka Jasiecka-Mikołajczyk[c], Bartosz Rasiński[d], Paweł Wojtacha[e]

[a]*Department of Chemistry, Faculty of Agriculture and Forestry, University of Warmia and Mazury in Olsztyn, Łódzki Square 4, 10-727 Olsztyn, Poland, emails: tomasz.mikolajczyk@uwm.edu.pl (T. Mikołajczyk), mateusz.luba@uwm.edu.pl (M. Łuba), mateusz.kuczynski@uwm.edu.pl (M. Kuczyński), bogpierozynski@yahoo.ca (B. Pierożyński)*
[b]*Łukasiewicz Research Network, Institute of Electrical Engineering, Mieczysława Pożaryskiego 28, 04-703, Warsaw, Poland, email: mateusz.luba@iel.lukasiewicz.gov.pl (M. Łuba)*
[c]*Department of Pharmacology and Toxicology, Faculty of Veterinary Medicine, University of Warmia and Mazury in Olsztyn, Oczapowskiego 13, 10-719 Olsztyn, Poland, email: agnieszka.jasiecka@uwm.edu.pl (A. Jasiecka-Mikołajczyk)*
[d]*Waters Corporation, Wybrzeze Gdynskie 6b, 01-531 Warszawa, Poland, email: bartosz_rasinski@waters.com (B. Rasiński)*
[e]*Department of Industrial and Food Microbiology, Faculty of Food Science, University of Warmia and Mazury in Olsztyn, Cieszyński Square 1, 10-726, Olsztyn, Poland, email: pawel.wojtacha@uwm.edu.pl (P. Wojtacha)*

Received 14 September 2022; Accepted 19 January 2023

**ABSTRACT**

Introduction of novel wastewater treatment technologies plays an important role in sustainability and environmental management. Commonly used wastewater purification processes are based on a combination of physical, chemical and biological methods. Despite their relatively good effectiveness in the removal of dyes, these treatments involve employment of various chemicals and biological additives, where their operational costs are very high. Thus, researchers continuously work to develop new ways of wastewater treatment, for example, electrochemical techniques. Unfortunately, a traditional electrochemical method for the removal of pollutants requires large amounts of electrical energy. Thus, in this work, we report a wastewater purification method carried-out through a continuous anodic dissolution of iron (mild steel) anode for artificially aerated Cu/Fe galvanic (macro-corrosion) cells and synthetically prepared industrial wastewater solutions. Electrochemical experiments were performed by means of a laboratory size electrolyzer reactor, where the electrocoagulation process along with surface-induced electrooxidation phenomena were examined for wastewater containing Disperse Red 167 (DR167) dye. The above was visualized through the employment of electrochemical (cyclic voltammetry and AC impedance spectroscopy techniques) and instrumental spectroscopy analyses. As a result, the total removal of DR167 azo dye from the synthetic wastewater solution (evaluated by means of UV-Vis spectroscopy) reached about 85% and 97% after 900 and 3,600 s, correspondingly.

*Keywords:* Electrocoagulation; Electro-oxidation; Fe sacrificial anode; Galvanic cell; Anodic dissolution; Synthetic wastewater treatment

* Corresponding author.

## 1. Introduction

The world's total production of textile dyes reaches 800,000 tons/y. Wide range of dyes applications in different industry sectors leads to the generation of large amounts of dyes-containing wastewater, responsible for an extensive list of environmental and health impacts [1,2]. Globally, industrial plants discharge up to 15% of totally used dyes in effluents, directly into water bodies. Among various textile dyes, particular attention should be paid to the so-called azo dyes. This specific group of colouring agents is characterized by one or more azo group(s) (–N=N–) [3–5]. Their relatively large concentration in hydric resources directly impacts living organisms of biosystem, as well as human health. Studies conducted in recent years have confirmed the toxicity, mutagenic and carcinogenic effects of some of the azo dyes and their metabolites [6–10].

Nowadays, the process of azo dyes removal can be divided into three categories: chemical and physical processes through, for example, membrane filtration, physical adsorption or coagulation with chemical additives [11–22] and biological methods based on the decolourization action, carried-out by specific microorganisms [23–27]. Conventional physiochemical methods are quite expensive and cannot completely remove azo dyes from wastewater. Moreover, they typically require metal salts or polymeric coagulants as destabilization agents that lead to undesirable water quality impairment. Thus, further wastewater treatment steps must be implemented. On the other hand, although biological methods are considered clean, they have their own, severe limitations, for example, relative low process's efficiency, as compared to physical or chemical methods and the requirement of large working areas [28].

On the other hand, in the last years, the DC-powered electrochemical methods have been utilized for the remediation of dye-polluted wastewaters. This method attracted a lot of attention because it may combine three simultaneously occurring processes: electrocoagulation, electrooxidation and electroflotation [29–31]. When the current is applied to the DC-powered electrochemical reactor, an anode undergoes the current-depending anodic dissolution. Therefore, the anode acts as a supplier of in situ created coagulant in the form of metal cations that immediately form its hydroxides with hydroxyl anions generated at the cathode surface. Such, in situ freshly produced hydroxide complexes act as destabilizing agent and lead to the formation of insoluble agglomerates with dye molecules that sediment on the bottom of sedimentation tank. Then, such formed solid layer could be siphoned out through the filtration process [32–35]. The process of electrochemical oxidation at the anode occurs in two different pathways: direct and indirect oxidation.

The main route of electrochemical oxidation would be direct oxidation, where pollutants present in the wastewater are oxidized directly on the anode surface. Then, the transfer of electrons is mediated by generated on the cathode hydroxyl radicals (•OH). Such short-lived species is considered a strongly oxidizing agent. Thus, the above process could lead to the azo bond dyes' cleavage and gradual degradation of dye molecules [36–39]. Electroflotation is the last of the processes mentioned above, which is strongly connected with electrochemical wastewater treatment. During the anodic process, oxygen bubbles are generated and released from the electrode surface. Simultaneously, at the cathode surface, hydrogen bubbles are formed as a result of the reduction process. The efficiencies of $H_2$ and $O_2$ formation is strictly dependent on the electrochemical activity of the electrode material and the applied current. Such-formed gas bubbles can carry the insoluble electrocoagulant-dye agglomerates into the surface of the reactor tank, where they could later be removed through mechanical methods [40–43]. Many studies reported that total decolourization of azo dyes-containing wastewater utilizing a DC-powered electrochemical system ranged between 71% and 99% [44–52]. Despite reasonably high efficiency of such DC-powered systems, they still suffer from high consumption of electrical energy, making it relatively non-profitable.

Development of novel, more efficient and cheaper, dye-based wastewater treatment methods, has become of superior technological importance in recent years. The electrochemical method based on the galvanic series theory may meet the above demands. An appropriately designed galvanic-cell reactor generates spontaneous current without using expensive DC-powered infrastructure, control systems, and does work without adding any other chemicals into the system. Hence, the total consumption of electricity and production of potentially dangerous by-products become radically limited. The profitability of using electrochemical methods based on the galvanic-cell theory was confirmed in the recently published work from this laboratory, where Cu/Al alloy galvanic macro-corrosion cell was employed for treatment of dye-based synthetic wastewater [53]. The results indicated that such-constructed cells provided sufficient currents to initiate electrocoagulation and electrooxidation processes with relatively high efficiency, without using external power sources or chemicals.

During the electrolysis process in the Cu/Fe reactor, the iron anode undergoes oxidation reaction and releases soluble ferrous ions ($Fe^{2+}$) that rapidly form its hydroxide species through the reaction with $OH^-$ ions generated on the surface of the cathode [54–57]. During the electrolysis process, electrolyte's pH becomes increased. The mechanism of the anodic and cathodic reactions for the Cu/Fe galvanic cell is described by Eqs. (1)–(3):

Anodic reaction:

$$Fe_{(S)} \rightarrow Fe^{2+} + 2e^- \tag{1}$$

Cathodic reaction:

$$O_2 + 2H_2O + 4e^- \rightarrow 4OH^- \tag{2}$$

Formation of ferrous hydroxide and ferric oxide:

$$2Fe^{2+} + 4OH^- \rightarrow 2Fe(OH)_{2(S)}\left(+\frac{1}{2}O_2\right) \rightarrow Fe_2O_{3(S)} + 2H_2O \tag{3}$$

Thus, Fe dissolution leads initially to the formation of ferrous hydroxide species [Eq. (3)] during the spontaneous reaction of $Fe^{2+}$ cations emerged in the supporting solution upon the anodic dissolution process [Eq. (1)] with hydroxyl ($OH^-$)

anions generated on the cathode surface [Eq. (2)]. Then, in the presence of dissolved oxygen, ferrous hydroxide becomes converted to ferric oxide ($Fe_2O_3$), according to Eq. (3).

The objective of this work was to evaluate the effectiveness of Cu/Fe galvanic cell's employment in the electrochemical wastewater treatment for artificially-prepared industrial wastewater, comprising small amounts of technologically important dye, namely Disperse Red 167 (DR167). The dye removal was made by means of the combined effect of electrocoagulation and surface-electrooxidation.

## 2. Materials and methods

### 2.1. Macro-galvanic cell reactor's construction and electrolysis process

In this work, the wastewater electrocoagulation/electrooxidation unit was composed of *ca.* 300 mL glass-made electrochemical reactor and electrodes, that are arranged in the way, where a single sacrificial anode is placed between two cathodes. A cylindrical shape low carbon steel was used as a sacrificial anode with an effective surface area of 29.3 $cm^2$ (diameter $\phi$ = 3.5 cm, thickness: $d$ = 1 cm): DIN C15 (1.0401; ArcelorMittal, Dąbrowa Górnicza, Poland), whereas a cathode was made of cylindrically-shaped copper with total effective electrode area of 84 $cm^2$ (two plates: 4 cm × 5 cm × 0.1 cm each). In the electrolyser unit, an inter-electrode (anode–to–cathode) gap was set at about 15 mm.

Before each series of experiments, the iron anode was cleaned off and polished by means of sandpaper, down to 2,500 grade. Such-precleaned anode was smooth and had a shiny silver colour. Then, the Fe electrode was submerged in 5% HCl solution for 5 min in order to allow its electrochemical activation. Finally, the anode was thoroughly rinsed with ultrapure water (18.2 MΩ/cm Millipore Q 3 UV Water Purification System manufactured by Millipore/Merck was used, Poznań, Poland). In the next step, the electrode was de-greased in pure ethanol. At the same time, both Cu cathodes were activated in 5% HCl, rinsed with ultrapure water and finally de-greased in ethanol. All experiments were performed at 293 ± 1 K.

During measurements of open-circuit voltage (ocv) and $I_{gc}$ parameters, the cell was operated with additional aeration (by slow purging of compressed oxygen to reach the value of *ca.* 10.5 ppm of dissolved oxygen). It should be noted that oxygen itself had completely no influence on the process of the dye oxidation (Fig. S1). However, prior and during the cyclic voltammogram and electrochemical impedance spectroscopy experiments, working solution was always de-aerated with high-purity argon (6.0 research grade Ar supplied by Linde) in order to prevent from spontaneous oxidation of the Fe electrode surface. In the electrochemical experiments, all electrode potentials were measured vs. saturated calomel electrode (SCE) reference electrode. Open-circuit voltages were always measured prior to and after completion of the electrochemical tests.

### 2.2. Solutions and chemicals

In order to assess the effectiveness of both electrocoagulation and electrooxidation processes, synthetic azo dye Disperse Red 167 (Boruta-Zachem SA, p.a.; Poland) solution was prepared. The procedure covered dissolving 50 mg/$dm^3$ of dye in $Na_2SO_4$-based supporting electrolyte (Polish Chemical Compounds, p.a.). In order to provide the required for the galvanic cell's operation, high effectiveness of the oxidation process and to avoid chemical coagulation, the solution's conductivity was set at about 15 mS and its pH was adjusted to the value of 4.5. Prior to and during the experiments, pH value for each solution was adjusted with dilute (0.1 M) sulphuric acid or sodium hydroxide solutions. HCl was not employed simply to avoid possible chlorination effects of aromatic pollutants that could normally be present in industrial wastewaters.

### 2.3. Experimental methodology

All electrochemical experiments (cyclic voltammetry and AC impedance spectroscopy tests) were performed at room temperature (298 ± 1 K) by means of Solartron 12,608 W Full Electrochemical System. Otherwise, electrolyte pH and conductivity evaluations were carried-out with HI 2002-01 and HI 9835 meters from Hanna Instruments, respectively. The electrochemical impedance spectroscopy measurements were performed at an AC signal of 5 mV over the frequency range swept between $1.0 \times 10^5$ and $0.5 \times 10^{-1}$ Hz, whereas cyclic voltammetry (CV) experiments were performed at a sweep-rate of 50 mV/s. In order to perform all the electrochemical experiments, the instruments were controlled by ZPlot 2.9 and CorrWare 2.0 software packages (Windows, Scribner Associates, Inc., Southern Pines, North Carolina, USA). All recorded cyclic voltammetry and impedance data were analyzed by ZView 2.9 and CorrView 2.9 software packages, respectively, where the impedance spectra were fitted with a complex, non-linear, least squares immittance fitting program LEVM 6, written by Macdonald [58]. Prior to electrochemical measurements, working electrode was cathodically polarized at –0.1 A for 600 s in pure 0.054 M $Na_2SO_4$ solution to remove the surface oxides formed during previous experiments. The CV characterization of low carbon steel electrode was conducted over the potential range: –1.1 to 0 V vs. SCE, commencing the sweep from the most negative electrode potential.

In order to monitor the progress of electrochemical treatment of the azo dye-containing wastewater over time, the solution samples were collected after 900; 1,800; 2,700 and 3,600 s of the Cu/Fe cell's continuous operation. Then, efficiency evaluation of the carried-out wastewater purification treatment was determined using a UV-Vis spectroscopic methods. The UV-Vis absorption spectra for the DR167 azo dye were recorded by means of the spectrophotometric plate reader Epoch 2 (BioTek, USA) on polystyrene plates (UV-Star® Microplates, Greiner Bio-One, Germany). The absorption spectra for all the collected samples were recorded for wavelengths between 230 and 800 nm. A degree of specific dye degradation was then assessed at all electrolysis times, namely: 0; 900; 1,800; 2,700 and 3,600 s. Such-obtained results were then analyzed with GraphPad Prism 6 Software (GraphPad, San Diego, CA, USA). The colour removal's efficiency ($\eta$) was calculated according to Eq. (4):

$$\eta = \frac{\left(C_0 - C_1\right)}{C_0} \cdot 100\% \tag{4}$$

where $C_0$ is an initial dye concentration and $C_1$ is the dye concentration after 3,600 s of treatment.

The chromatographic quantitation of the DR167 level was achieved in reversed-phase liquid chromatography system ACQUITY UPLC (ultra-performance liquid chromatography) I-Class PLUS, coupled with a Xevo TQ-XS Triple Quadrupole mass spectrometry (Waters, Milford, USA). Chromatographic separation of the DR167 dye was achieved on ACQUITY UPLC HSS T3 column (1.8 μm; 2.1 mm × 100 mm; Waters) maintained at 40°C. The mobile phase consisted of phase A (0.1% citric acid in water) and phase B (0.1% citric acid in acetonitrile) in the gradient elution. Each analysis was carried-out for 5 min and the flow rate of 400 μL/min was used for the sample analysis. The injection volume was 1 μL and the temperature of the autosampler was maintained at 15°C. Detection was performed with double quadruple Tandem mass spectrometry in the positive ion mode, where the setting parameters of the detector are presented in Table 1. Equipment was set up in a multiple reaction monitoring (MRM) mode and transitions from 506.16 → 249.1 m/z, 506.16 → 446.14 m/z and 506.16 → 464.14 m/z were used for pigment determination. The final computations for the DR167 were conducted based on 506.16 → 249.1 m/z transition. Samples collected from the electrolysis cell (10 μL) were dissolved in water to achieve a final volume of 500 μL and transferred into total recovery vials (Waters). An aliquot was then injected for liquid chromatography-Tandem mass spectrometry analysis. The obtained chromatographic data were analyzed by MassLynx and TargetLynx software packages.

## 3. Results and discussion

### 3.1. Characterization of macro-corrosion, galvanic cell's operation

The electrochemical characterization of the Cu/Fe mild steel galvanic cell was carried-out in $Na_2SO_4$ supporting electrolyte (pH = 4.5 for DR167-based solution; κ = 10.0 mS/cm: 0.054 M $Na_2SO_4$, 10.5 ppm of dissolved oxygen and $T$ = 20°C). It could be seen that after an hour of continuous operation, an open-circuit voltage (ocv) under open cell conditions reached a steady state value of 0.64 V for synthetically prepared wastewater solution with DR167 (Fig. 1).

Table 1
Tandem mass spectrometric (MS/MS) parameters for the determination of DR167

| MS/MS parameters | |
|---|---|
| Precursor ion (m/z) | 506.16 |
| Product ions (m/z) | 249.1; 446.14; 464.14 |
| Desolvation gas | Nitrogen |
| Desolvation gas temperature (°C) | 350 |
| Desolvation gas flow (L/h) | 300 |
| Cone gas flow (L/h) | 150 |
| Collision gas | Argon |
| Source temperature (°C) | 120 |
| Electrospray mode | Positive |
| Cone voltage (V) | 20 |
| Capillary voltage (kV) | 3.0 |
| Retention time (min) | 2.2 |

The Cu/Fe macro-galvanic cell's electrochemical performance was examined by measuring the galvanic coupling current ($I_{gc}$). The determination of $I_{gc}$ values in examined solution plays a crucial role because current (or current-density) is a parameter that controls the rate of electrochemical reactions which occur in a galvanic macro-corrosion cell. Hence, after 1 h of continuous work of the Cu/Fe galvanic cell (Fig. 2), the recorded $I_{gc}$ value came to 6.80 mA (0.23 mA/cm) for DR167-dye-based solution (and resulted in an anode loss at a rate of *ca.* 0.03 wt.% per hour).

In addition, rising concentration of $Fe^{2+}$ ions in the working solution, in the presence of dissolved oxygen, would also lead to the spontaneous formation of coagulation agent – ferric hydroxide: $Fe(OH)_3$ species [Eq. (5)] that could bind to the pollutant molecules. Hence, freshly formed iron(III) hydroxide species would attract oppositely charged dye molecules, leading to charge neutralization, destabilization and then formation of larger agglomerates that eventually sediment on the bottom of the reaction tank. Such coagulation agent-pollutant agglomerates could later be removed through siphoning them off the reactor tank by filtration process. On the other hand, the anodic surface oxidation process might simultaneously induce degradation of surface-adsorbed dye entity to form simpler molecules. In fact, the above-described mechanism is in full agreement with available scientific literature for DC-powered iron-based wastewater electrocoagulation process [59–61].

$$4Fe^{2+} + 10H_2O + O_2 \rightarrow 4Fe(OH)_{3(S)} + 8H^+ \quad (5)$$

### 3.2. Cyclic voltammetry

The electrochemical behaviour of low carbon steel electrode in 0.054 M $Na_2SO_4$ supporting solution was initially examined by means of cyclic voltammetry (CV) technique, over the potential range: –1.1 to 0.0 V vs. SCE. Fig. 3 shows the second cycle of the cyclic voltammetry response for the iron working electrode of the Cu/Fe galvanic cell, carried-out in pure and DR167-based 0.054 M $Na_2SO_4$ supporting electrolyte, obtained at 293 K with a sweep-rate of 50 mV/s.

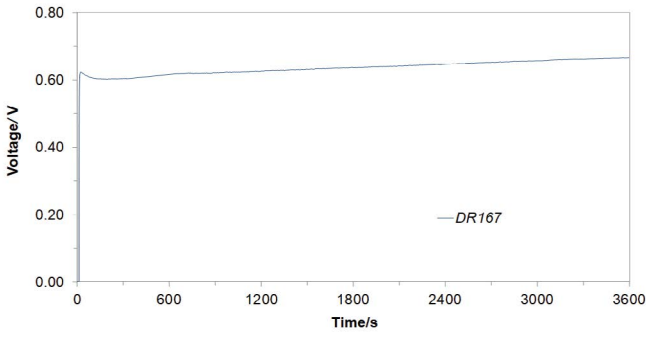


Fig. 1. Recorded value of open-circuit voltage in time for Cu/Fe macro-galvanic cell, derived for freshly-prepared, DR167-containing (50 mg/dm$^3$) $Na_2SO_4$-based solution.

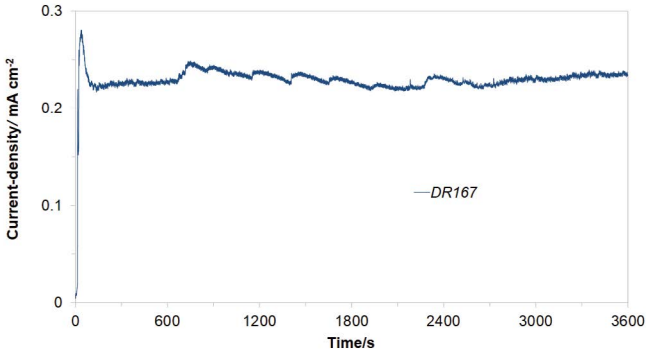


Fig. 2. Recorded galvanic couple current-density for macro-corrosion Cu/Fe galvanic cell in function of exposure time, derived for freshly-prepared, aerated DR167-containing (50 mg/dm$^3$) $Na_2SO_4$-based solution (the Fe anode potential oscillated around 600 mV vs. saturated calomel electrode).

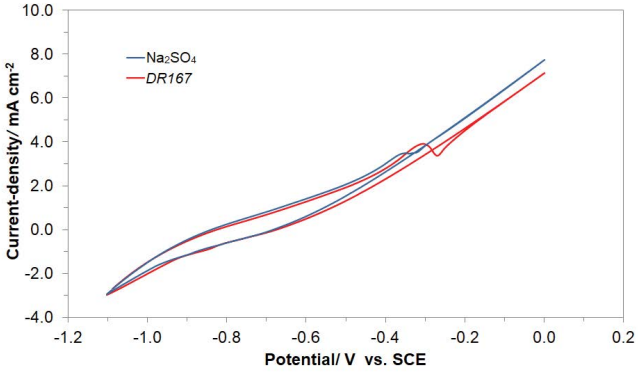


Fig. 3. Cyclic voltammetry for macro-corrosion Cu/Fe galvanic cell in the presence and absence of DR167 dye in $Na_2SO_4$-based solution, recorded for the second CV sweep at a scan rate of 50 mV/s (extended voltage range to 0.8 V cyclic voltammogram is also presented in Fig. S3).

For the cyclic voltammogram obtained in the absence of DR167 dye, two irreversible anodic peaks could be observed, namely: one very broad feature centered at *ca.* –0.85 and another positioned at –0.36 V vs. SCE. Both peaks are generally believed to be due to the anodic dissolution of low carbon steel electrode to produce $Fe^{2+}$ and $Fe^{3+}$ cations. The former low potential anodic peak might correspond to the process of Fe(II) formation, whereas the latter one might be assigned to its further oxidation to $Fe_3O_4$ or formation of $Fe(OH)_3$ [62–64]. A majority of such-generated insoluble compounds would eventually sediment at the bottom of the reaction tank.

Then, in the presence of the DR167 dye, similarly to the behaviour observed in pure $Na_2SO_4$ solution, two irreversible anodic reaction patterns are still observed. However, the second, high potential anodic feature is now significantly broader and shifted towards more positive potentials, with the peak's centre located at –0.30 V (Fig. 3). Here, this peak could most likely be associated with a combined oxidation of electrode surface and the –N=N– azo group in the examined dye [65–68]. The above is in-line with a radical increase of the peak's current-density (charge), as seen in the cyclic voltammetric feature of Fig. 3. In addition, it should be noted that the combined chromatography/mass spectrometry analysis carried-out on the electrolyte sample obtained via the continuous voltammetric cycling (100 cycles, restricted to the potential range of the above-mentioned peak) produced a number of the DR167 surface electrodegradation products (Fig. S2).

### 3.3. Electrochemical impedance characterization

The ac. impedance characterization of low carbon steel electrode's reactivity in pure $Na_2SO_4$ and in the presence of DR167 dye in the supporting solution is shown in Table 2 and Fig. 4a through 6c below. Hence, at the most negative potentials (–900 to –800 mV vs. SCE), the Nyquist impedance spectra exhibited two "depressed", partial semicircles, clearly discernible in the impedance plots (Fig. 4a). Here, a circuit model containing two time constants (CPE: constant phase element-modified, Fig. 5a) was employed to characterize the recorded impedance behaviour. The high-frequency semicircle is associated with Fe(II) formation (electrode dissolution process), whereas the low-frequency arc corresponds to the adsorption of $Fe(OH)_2$ layer on the electrode surface. The iron(II) hydroxide is formed during the electrolysis process from $Fe^{2+}$ cations derived from the anode and $OH^-$ hydroxyl anions are generated on the Cu cathode surface during the oxygen reduction reaction [Eq. (2)] [54–57,62].

On the other hand, at positive potentials to –800 mV (–390 to –280 mV), only one somewhat depressed semicircle was noticed in relation to a single-step charge transfer reaction (examples of this behaviour in Fig. 4b and c). However, as argued based on the CV characterization above, for the dye-containing solution, this potential range should cover two (electrode and pigment), parallel surface oxidation/degradation processes. Hence, a circuit model (Fig. 5b) used for fitting the latter data (except for the dye-based synthetic wastewater, recorded at the potential of –330 mV, Fig. 5c) contained only one time constant. The CPE element is included in the equivalent circuits in order to account for the so-called capacitance dispersion [69], due to the surface heterogeneity effect. The above is caused by increased roughness of the electrode surface along with the effect of adsorption of impurities, being able to form porous layers on the electrode surface [70]. Here, the impedance response is associated with further electrode surface oxidation process, resulting in the formation of Fe(III) species [64].

Thus, for the first, broad oxidation peak, centred at about –850 mV vs. SCE, the recorded charge-transfer resistance ($R_{ct}$) parameter came to 103.6 and 72.9 Ω/cm$^2$ (at –850 mV) for pure $Na_2SO_4$ and the DR167 dye-modified electrolyte, respectively. This indicates that the presence of an azo dye molecule in the working solution did significantly impact the Fe(II) formation during the anodic dissolution process. The latter could also be supported by significant reduction of the interfacial capacitance parameter ($C_{dl}$) from 1,828 (in dye-free solution) to 1,609 μF/cm$^2$, recorded in the presence of the DR167 dye.

Furthermore, the recorded average adsorption charge-transfer resistance ($R_{Ads}$) value oscillated around 3,270 and 1,490 Ω/cm$^2$ for pure and the DR167 dye-based wastewater solution, correspondingly, over the examined

Table 2
Parameters for the processes of Fe electrode oxidation and azo dye electrodegradation (at a total concentration of DR167 at 50 mg/dm$^3$) on the surface of Fe mild steel anode in contact with 0.054 M $Na_2SO_4$, achieved by fitting equivalent circuit models presented in Fig. 5a–c to the experimentally-obtained impedance data [dimensionless $\phi$ parameter, which determines the constant phase angle in the complex-plane plot ($0 \le \phi \le 1$) of the constant phase elements circuit, varied between 0.67 and 0.86, and 0.54 and 0.87 for $\phi_1$ and $\phi_2$, respectively]

| $E$ (mV) | $R_{ct}$ (Ω/cm$^2$) | $C_{dl}$ (μF/cm$^2$·s$^{\cdot\phi 1-1}$) | $R_{Ads}$ (Ω/cm$^2$) | $C_{Ads}$ (μF/cm$^2$·s$^{\cdot\phi 2-1}$) |
|---|---|---|---|---|
| | | $Na_2SO_4$ | | |
| –900 | 76.2 ± 6.7 | 2,920 ± 263 | 3,775 ± 416 | 7,853 ± 292 |
| –850 | 72.9 ± 3.2 | 1,828 ± 116 | 3,190 ± 347 | 9,763 ± 112 |
| –800 | 62.4 ± 1.4 | 958 ± 41 | 2,846 ± 33 | 9,563 ± 57 |
| –390 | 22.8 ± 0.1 | 1,543 ± 31 | – | – |
| –360 | 22.0 ± 0.1 | 882 ± 20 | – | – |
| –330 | 15.3 ± 0.1 | 664 ± 15 | – | – |
| –300 | 19.7 ± 0.1 | 655 ± 13 | – | – |
| –280 | 19.5 ± 0.1 | 684 ± 17 | – | – |
| | | DR167 dye | | |
| –900 | 77.6 ± 2.0 | 1,230 ± 43 | 1,321 ± 103 | 13,239 ± 258 |
| –850 | 103.6 ± 4.5 | 1,609 ± 140 | 1,548 ± 134 | 11,451 ± 260 |
| –800 | 83.6 ± 5.4 | 923 ± 98 | 1,612 ± 209 | 9,567 ± 186 |
| –390 | 15.6 ± 0.2 | 2,194 ± 96 | – | – |
| –360 | 11.3 ± 0.1 | 2,061 ± 97 | – | – |
| –330[a] | 8.8 ± 0.1 | 1,374 ± 63 | 4.7 ± 0.8 ($R_F$) | 6,614 ± 1,198 ($C_P$) |
| –300 | 8.9 ± 0.1 | 1,628 ± 65 | – | – |
| –280 | 8.6 ± 0.1 | 1,721 ± 77 | – | - |

[a]Fig. 5c for details.

potential span. The above could suggest that the presence of the dye (or its degradation by-products) in solution could facilitate the formation of $Fe(OH)_2$. Analogously, the recorded average pseudocapacitance ($C_{Ads}$) parameter value for the dye-based solution was significantly increased (11,420 μF/cm$^2$), as compared to that derived for the dye-free solution (9,060 μF/cm$^2$).

Then, the recorded $R_{ct}$ parameter for the second oxidation peak, at the potential of –360 mV vs. SCE for pure $Na_2SO_4$ and the DR167-based solutions came to about 22.0 and 11.3 Ω/cm$^2$, respectively. This difference is most likely caused by significant surface expansion effect, incurred upon the DR167 dye adsorption (along with its degradation by-products) on the surface of mild steel electrode. Hence, the $C_{dl}$ parameter values obtained in pure and the DR167-modified $Na_2SO_4$ solution at the potential of –360 mV came to about 882 and 2,061 μF/cm$^2$, correspondingly. In fact, the $C_{dl}$ parameter is closely related to the size/thickness of the formed Fe(III) surface layer [62–64].

However, in the presence of the DR167 dye, the Nyquist impedance spectrum exhibited two "depressed", partial semicircles (Fig. 4c and additional Bode plot – Fig. S4), at the potential of –330 mV. The high-frequency semicircle is associated with the oxidation of Fe(II) surface layer to form Fe(III) adlayer, whereas the low-frequency arc corresponds to the dye's oxidative degradation. Thus, the data were fitted with two CPE-R element equivalent circuit (Fig. 5c). Here, the recorded $R_{ct}$ parameter reached the value of 8.8 Ω/cm$^2$, which was 1.7 × smaller, as compared to that recorded at the same potential, but in unmodified $Na_2SO_4$ solution. Also, the recorded $C_{dl}$ parameter was twice as high as that derived for pure sulphate salt working solution. Most importantly, the recorded Faradaic charge-transfer resistance, $R_F$ parameter, associated with an initial stage of the degradation, reached 4.7 Ω/cm$^2$, while the corresponding pseudocapacitance, $C_P$ value reached 6,614 μF/cm$^2$. Unfortunately, at other examined potential values over the range: –390 to –280 mV, the processes of electrode surface oxidation and the dye degradation could not be separated from the impedance spectra.

### 3.4. UV-Vis spectrophotometry analysis

In this work, the process of Fe surface electrooxidation and electrodegradation of the examined azo dye upon the operation of the Cu/Fe galvanic macro-corrosion cell was monitored by utilizing UV-Vis spectrophotometry technique, where process's optimization was carried-out by recording absorption spectra over 230–800 nm wavelength range.

It is well-known that the process of azo dye oxidation or degradation can be divided into three consecutive stages: decolourization (break of the azo bond in the dye molecule), degradation of benzene ring in the dye molecule and complete or partial mineralization process that could be visualized by absorbance changes within the UV-Vis spectrum for the selected wavelength ranges of 350–600, 267–350 and 200–265 nm, respectively.

During the electrolysis process (dissolution of iron mild steel anode), the azo dye underwent electro-oxidation and electrocoagulation processes, which could be confirmed by the obtained spectrophotometric results.

Hence, UV-Visible absorption spectra of DR167 dye-based (50 mg/dm$^3$) wastewater solution, recorded at different electrolysis times are shown in Fig. 6a. They indicated that the DR167 dye underwent electrooxidation process, which led to the formation of products different in structure. These results also implied significant concentration depletion of the dye molecules.

Fig. 6b and c show an increase in the absorbance values for the wavelengths of 470 and 280 nm during an initial 900 s of the electrolysis. With respect to both, azo bond and aromatic ring degradation stage, the above is most likely associated with the destruction of an initial form of the dye molecule into different products (e.g., aromatic/phenol and aromatic amine derivatives that are structurally similar to 3-amino-2-hydroxy-5-nitrobenzenesulfonic acid or 2-chloro-4-nitrobenzamine) containing both azo bond and aromatic ring in their structure [53]. Interestingly, after 900 s of continuous electrolysis, no further changes in the products' structure were observed (Fig. 6b and c). The initial stage of the DR167 degradation is most likely associated with its intramolecular rearrangements that lead to the formation of products having somewhat different structure. In this case, one of the nitrogen atoms from the azo bond, aromatic ring or delocalized $\pi$ electron cloud might act as an electron acceptor. The results obtained from the absorbance measurement at 240 nm indicated no sign of multimerization during the electrolysis of the DR167 dye (Fig. 6d). It has to be stated here that the removal of the azo dye involved a combination of two steps, namely: surface electrooxidation and electrocoagulation processes, yielding calculated dye removal level on the order of 85% and 96% after 900 and 3,600 s (Fig. 6e), respectively.

### 3.5. Chromatography

The total dye removal was also evidenced by ultra-performance liquid chromatography coupled with double quadruple Tandem mass spectrometry (UPLC-MS/MS) analysis, which showed that after 900 s and 3,600 s of continuous

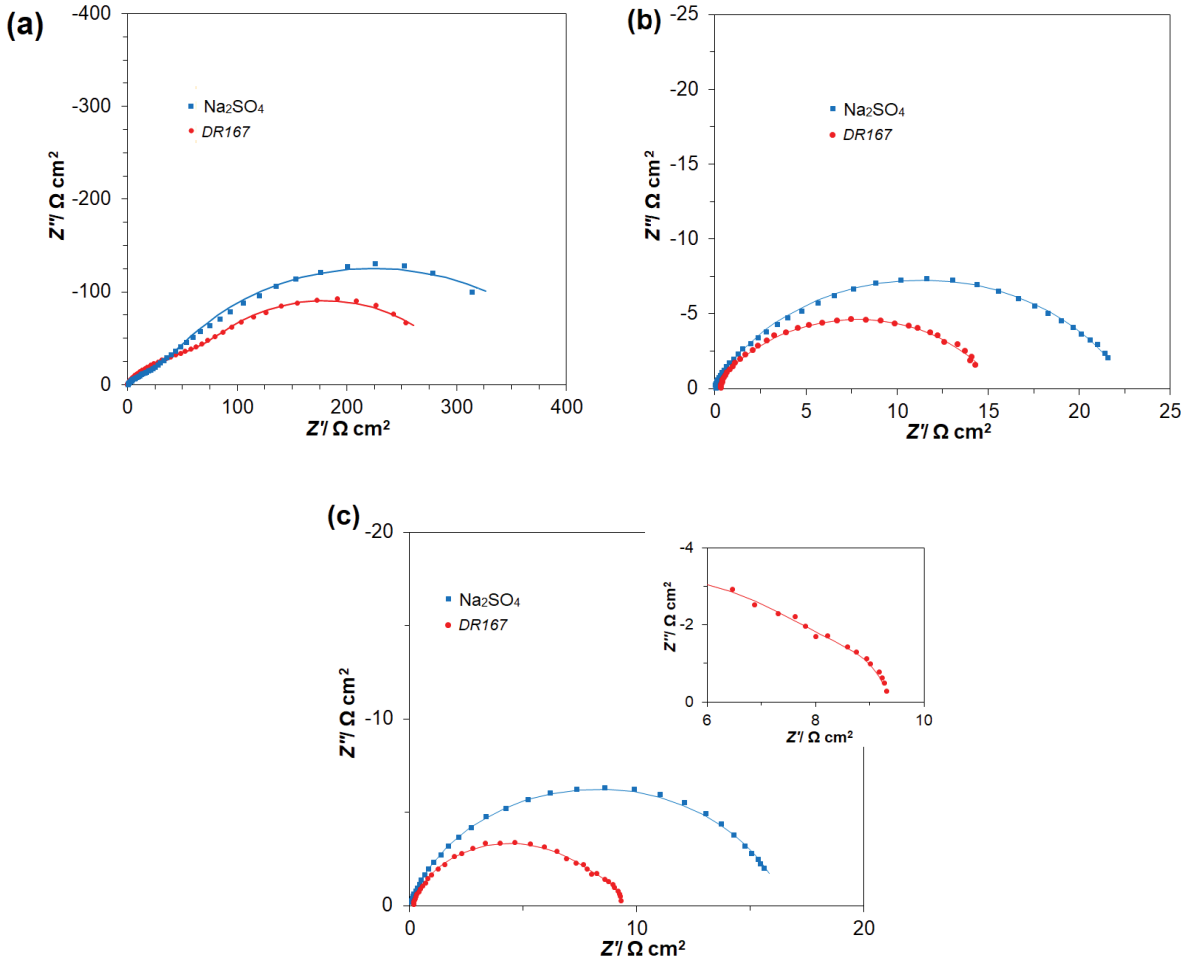


Fig. 4. The recorded complex plane Nyquist impedance plots for Fe mild steel electrode in contact with pure 0.054 M $Na_2SO_4$ and DR167-modified (50 mg/dm$^3$) $Na_2SO_4$ solution, derived for the following potentials: (a) –900, (b) –390 and (c) –330 mV vs. saturated calomel electrode. The solid lines correspond to the representation of the data according to the equivalent circuit models presented in Fig. 5a–c, respectively.

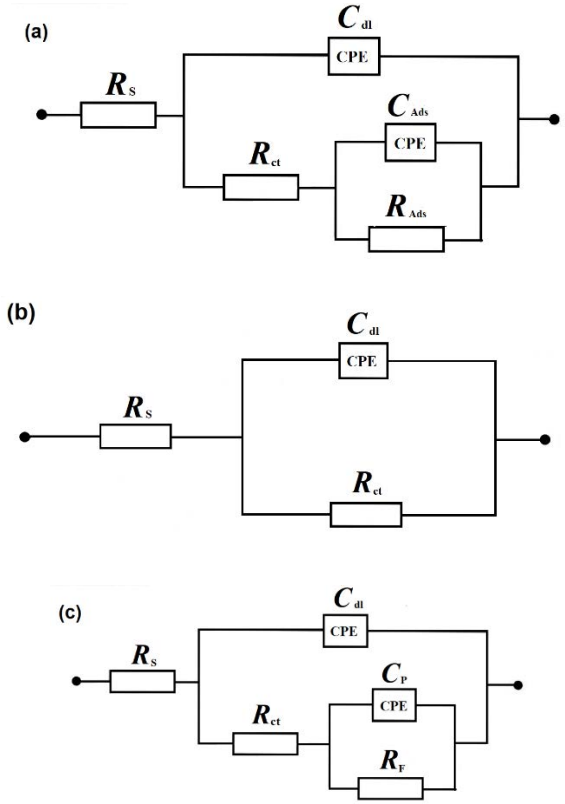


Fig. 5. Three equivalent circuits, used for fitting the obtained AC impedance spectroscopy data, where $R_s$ is solution resistance; $C_{dl}$ is double-layer capacitance; $R_{ct}$ is charge-transfer resistance parameter for electrooxidation of Fe anode surface; $R_{Ads}$ and $C_{Ads}$ are adsorption resistance and capacitance parameters for $Fe(OH)_2$ film; $R_F$ and $C_P$ are Faradaic charge-transfer resistance and pseudocapacitance parameters, connected with oxidative degradation of DR167 dye molecule, respectively. The circuits include constant phase elements to account for distributed capacitance.

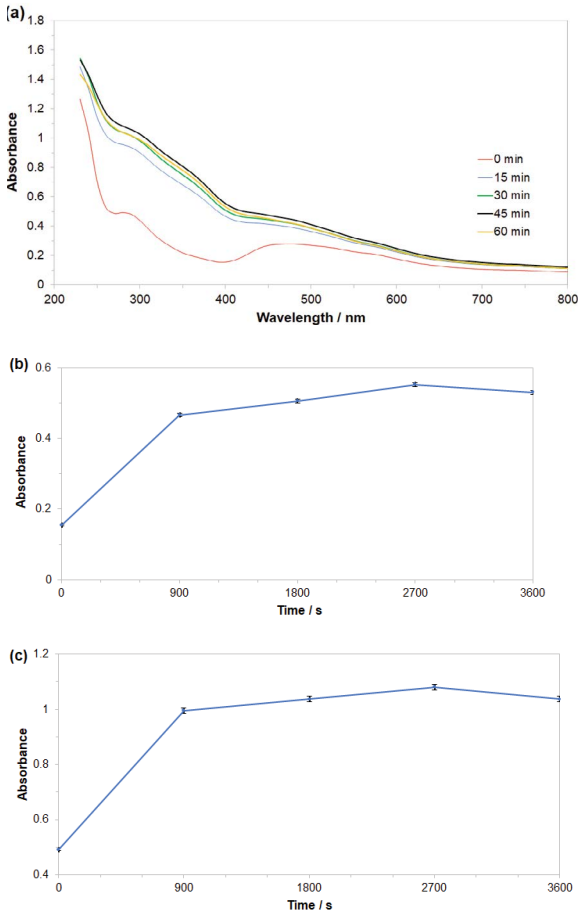


Fig. 6. UV-Vis spectra changes of DR167 dye at different times of wastewater treatment for Cu/Fe macro-corrosion galvanic cell, where: (a) representation of the three stages of dye electrooxidation process on the surface of Fe anode in $Na_2SO_4$-based DR167 solution (at the concentration of 50 mg/dm$^3$), (b) evolution of decolourization process recorded for the wavelength of 470 nm, (c) progress of aromatic ring degradation for the wavelength of 280 nm, (d) evolution of mineralization process recorded for the wavelength of 240 nm, and (e) quantitative dye assay after sedimentation process for the wavelength of 470 nm.

electrolysis, the total removal of the dye came to 98% and over 99%, respectively (Table 3 and Fig. 7). Compared to the UV-Vis technique, there were noticeable differences in the obtained results. These discrepancies could be caused by the sheer differences between these methods, as the UPLC-MS/MS analysis is more selective than the UV-Vis spectrophotometry. Thus, the use of UPLC-MS/MS method allows to obtain the results of actual content of the examined dyes, compared to the estimated values given by means of the UV-Vis technique. Moreover, some of the coloured derivatives emerging during the dye electrolysis could not be distinguished from an initial substance through the UV-Vis analysis.

The decrease of the value of absolute peak height parameter (from $1.35 \times 10^8$ to $2.38 \times 10^5$) is strictly correlated to that observed in the value of the peak area. Thus, the percentage reduction of the dye based on both parameters, presented in Fig. 7 and Table 3, would be similar. In the representative chromatogram of the solution recorded after the electrolysis, a slight noise is observed around the retention time of 2.00 min, apart from the main peak of the DR167 dye. It is believed that this is a response from the by-products arisen during the electrolysis. Fig. S5 in the supplementary materials presents a scan of the above-mentioned noise with masses and retention times of potential dye derivatives produced during the electrolysis. As the process of

Table 3
Variation of the detected chromatographic peak area for DR167 substrate in time of electrolysis

| Electrolysis time (min) | Peak area |
|---|---|
| 0 | 1,927,556 ± 157,737 |
| 15 | 33,691 ± 3,007 |
| 30 | 24,827 ± 2,686 |
| 45 | 19,034 ± 753 |
| 60 | 12,115 ± 2,023 |

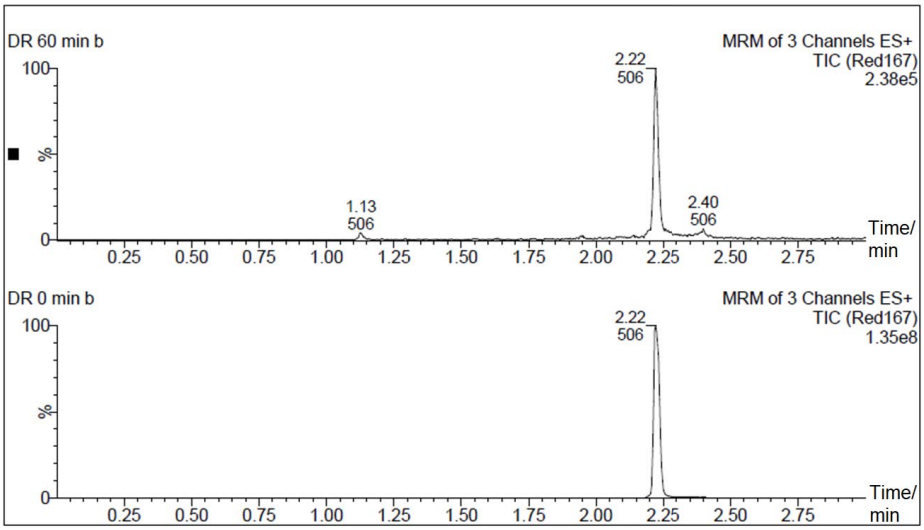


Fig. 7. Representative UPLC-MS/MS chromatograms for DR167, before and after 60 min of continuous electrolysis.

electrolysis causes accumulation of small amounts, but high molecular mass compounds, it could be concluded that initial breaking of the –N=N– azo bond leads to the formation of different, easily coagulating chemicals.

## 4. Conclusions

The electrochemical method for Disperse Red 167 azo dye-based wastewater purification, proposed in this work, gave very promising results. The employment of Cu/Fe mild steel macro-corrosion galvanic couple resulted in the removal of pigment through a combination of electrocoagulation and electrooxidation processes. Such-proposed electrochemical reactor was constructed based on the theory of galvanic series, where mild steel was employed as cheap and environmentally abundant material to make a sacrificial anode. Thus, Cu/Fe galvanic cell reactor was employed as a replacement for expensive to maintain external power source's infrastructure, which makes this method much more cost-effective than traditional DC-driven electrochemical approaches.

The UV-Vis and UPLC-MS/MS characterizations implied that the very complex in chemical structure DR167 pigment underwent oxidative destruction of its chemical formula, leading to the formation of numerous (although extremely hard to qualitatively identify) electrodegradation products. These products also experienced electrocoagulation process, which practically led to the total removal of the DR167 dye from wastewater solution (*ca.* 97 and over 99% for UV-Vis and UPLC-MS/MS methods, correspondingly). In addition, the existence of surface electrooxidation reactions was strongly supported by the recorded ac. impedance and cyclic voltammetry results.

In summary, the proposed here wastewater treatment method based on the operation of macro-corrosion galvanic cell may be considered a suitable replacement for the commonly used, multi-step wastewater treatment methods. However, further work is required in order to improve its overall effectiveness and durability.

## Symbols

| | | |
|---|---|---|
| AC | — | Alternating current |
| $C_0$ | — | Initial concentration |
| $C_1$ | — | Concentration after treatment |
| $C_{Ads}$ | — | Adsorption capacitance |
| $C_{dl}$ | — | Double-layer capacitance |
| $C_P$ | — | Pseudocapacitance |
| CPE | — | Constant phase element |
| CV | — | Cyclic voltammetry |
| DR167 | — | Disperse Red 167 |
| $I_{gc}$ | — | Galvanic coupling current |
| LC-MS/MS | — | Liquid chromatography with Tandem mass spectrometry |
| MRM | — | Multiple reaction monitoring |
| ocv | — | Open-circuit voltage |
| ppm | — | Parts per million |
| $R_{Ads}$ | — | Adsorption resistance |
| $R_{ct}$ | — | Charge-transfer resistance |
| $R_F$ | — | Faradaic charge-transfer resistance |
| SCE | — | Saturated calomel electrode |
| UPLC-MS/MS | — | Ultra-performance liquid chromatography with Tandem mass spectrometry |
| UV-Vis | — | Ultraviolet–visible spectroscopy |

## Patents

Pierożyński, B.; Smoczyński, L. Electrocoagulator for wastewater treatment, Patent of the Republic of Poland, PAT.227874, granted on 5 September 2017.

## Author contributions

Conceptualization, B.P.; methodology, B.P.; investigation, M.L., T.M., M.K., A.J-M., B.R. and P.W.; data curation, T.M., M.L. and M.K.; writing—original draft preparation, M.L.; editing, B.P. and T.M. All authors have read and agreed to the published version of the manuscript.

**Funding**

This work has been financed by the internal research grant no. 30.610.001-110, provided by The University of Warmia and Mazury in Olsztyn. The project was also supported by the grant no. 15.610.008-110, provided by the University of Warmia and Mazury in Olsztyn.

**Acknowledgments**

This paper stems from works related to the project No. WATERWORKS2017/1/WATER HARMONY/2/2019 (Closing the Water Cycle Gap with Harmonised Actions for Sustainable Management of Water Resources) financed by NCBR-Poland.

Mateusz Łuba would also like to acknowledge a scholarship from the program Interdisciplinary Doctoral Studies in Bioeconomy (POWR.03.02.00-00-1034/16-00), funded by the European Social Fund.

**Conflicts of interest**

The authors declare no conflict of interest.

**References**

[1] M.A. Hassaan, A. El Nemr, Health and environmental impacts of dyes: mini review, Am. J. Environ. Sci. Eng., 3 (2017) 64–67.
[2] M. Yusuf, Chapter 2 – Synthetic Dyes: A Threat to the Environment and Water Ecosystem, M. Shabbir, Ed., Textiles and Clothing: Environmental Concerns and Solutions, 1st ed., Scrivener Publishing LLC, New York, 2019, pp. 11–26.
[3] B. de Campos Ventura-Camargo, M.A. Marin-Morales, Azo dyes: characterization and toxicity – a review, Text. Light Ind. Sci. Technol., 2 (2013) 85–103.
[4] S. Benkhaya, S. M'rabet, A. El Harf, Classifications, properties, recent synthesis and applications of azo dyes, Heliyon, 6 (2021) e03271, doi: 10.1016/j.heliyon.2020.e03271.
[5] D. Rawat, R.S. Sharma, S. Karmakar, L.S. Arora, V. Mishra, Ecotoxic potential of a presumably non-toxic azo dye, Ecotoxicol. Environ. Saf., 148 (2018) 528–537.
[6] K.-T. Chung, Azo dyes and human health: a review, J. Environ. Sci. Health., Part C Environ. Carcinog. Ecotoxicol. Rev., 34 (2016) 233–261.
[7] A. Bafana, D.S. Saravana, T. Chakrabarti, Azo dyes: past, present and the future, Environ. Rev., 19 (2011) 350–370.
[8] B. Lellis, C.Z. Fávaro-Polonio, J.A. Pamphile, J.C. Polonio, Effects of textile dyes on health and the environment and bioremediation potential of living organisms, Biotechnol. Res. Innovation, 3 (2021) 275–290.
[9] T. Platzek, C. Lang, G. Grohmann, U.-S. Gi, W. Baltes, Formation of a carcinogenic aromatic amine from an azo dye by human skin bacteria in vitro, Hum. Exp. Toxicol., 18 (1999) 552–559.
[10] J. Feng, C.E. Cerniglia, H. Chen, Toxicological significance of azo dye metabolism by human intestinal microbiota, Front. Biosci. (Elite Ed.), 4 (2021) 568–586.
[11] E.K. Tetteh, S. Rathilal, M. Chetty, E.K. Armah, D. Asante-Sackey, Treatment of Water and Wastewater for Reuse and Energy Generation-Emerging Technologies, M. Eyvaz, Ed., Water and Wastewater Treatment, 1st ed., InTechOpen, London, 2019, pp. 1–22.
[12] N.E. Abdel-Raouf, N.E. Maysour, R.K. Farag, A.R.M. Abdul-Raheim, Wastewater treatment methodologies, review article, Int. J. Environ. Agric. Sci., 3 (2019) 1–25.
[13] J. Quach-Cu, B. Herrera-Lynch, C. Marciniak, S. Adams, A. Simmerman, R.A. Reinke, The effect of primary, secondary, and tertiary wastewater treatment processes on antibiotic resistance gene (ARG) concentrations in solid and dissolved wastewater fractions, Water, 10 (2018) 1–18.
[14] C.P. Gerba, L. Pepper, Municipal Wastewater Treatment, M.L. Brusseau, I.L. Pepper, C.P. Gerba, Eds., Environmental and Pollution Science, 3rd ed., Elsevier, San Diego, 2019, pp. 393–418.
[15] G. Crini, E. Lichtfouse, Advantages and disadvantages of techniques used for wastewater treatment, Environ. Chem. Lett., 17 (2019) 145–155.
[16] H. Zhou, D.W. Smith, Advanced technologies in water and wastewater treatment, J. Environ. Eng. Sci., 1 (2002) 247–264.
[17] G.Z. Kyzas, K.A. Matis, Wastewater treatment processes: Part I, Processes, 8 (2020) 334, doi: 10.3390/pr8030334.
[18] A. Demirbas, G. Edris, W.M. Alalayah, Sludge production from municipal wastewater treatment in sewage treatment plant, Energy Sources Part A, 39 (2017) 999–1006.
[19] A. Ahmad, S.H. Mohd-Setapar, S.C. Chuo, A. Khatoon, W.A. Wani, R. Kumar, M. Rafatullah, Recent advances in new generation dye removal technologies: novel search of approaches to reprocess wastewater, RSC Adv., 5 (2021) 30801–30818.
[20] S. Sharma, R. Saxena, G. Gaur, Study of removal techniques for azo dyes by biosorption: a review, IOSR - J. Appl. Chem., 7 (2014) 6–21.
[21] M.P. Shah, Azo dye removal technologies, Austin. J. Biotechnol. Bioeng., 5 (2018) 1–6.
[22] M. Chen, W. Ding, J. Wang, G. Diao, Removal of azo dyes from water by combined techniques of adsorption, desorption, and electrolysis based on a supramolecular sorbent, Ind. Eng. Chem. Res., 52 (2013) 2403–2411.
[23] N.Y. Donkadokula, A.K. Kola, I. Naz, D. Saroj, A review on advanced physico-chemical and biological textile dye wastewater treatment techniques, Rev. Environ. Sci. Biotechnol., 19 (2020) 543–560.
[24] R.G. Saratale, G.D. Saratale, J.S. Chang, S.P. Govindwar, Bacterial decolorization and degradation of azo dyes: a review, J. Taiwan Inst. Chem. Eng., 42 (2011) 138–157.
[25] A. Chen, B. Yang, Y. Zhou, Y. Sun, C. Ding, Effects of azo dye on simultaneous biological removal of azo dye and nutrients in wastewater, R. Soc. Open Sci., 5 (2018) 1–9.
[26] O. Türgay, G. Ersöz, S. Atalay, J. Forss, U. Welander, The treatment of azo dyes found in textile industry wastewater by anaerobic biological method and chemical oxidation, Sep. Purif. Technol., 79 (2021) 26–33.
[27] P.K. Singh, R.L. Singh, Bio-removal of azo dyes: a review, Int. J. Appl. Sci. Biotechnol., 5 (2021) 108–126.
[28] V. Karthik, K. Saravanan, P. Bharathi, V. Dharanya, C. Meiaraj, An overview of treatments for the removal of textile dyes, J. Chem. Pharm. Sci., 7 (2014) 301–307.
[29] Y. Feng, L. Yang, J. Liu, B.E. Logan, Electrochemical technologies for wastewater treatment and resource reclamation, Environ. Sci. Water Res. Technol., 2 (2016) 800–831.
[30] G. Chen, Y.T. Hung, Electrochemical Wastewater Treatment Processes, Humana Handbook of Environmental Engineering, L.K. Wang, Y.-T. Hung, N.K. Shammas, Eds., Advanced Physicochemical Treatment Technologies, 1st ed., Humana Totowa, New Jersey, 2007, pp. 57–106.
[31] C.A. Martinez-Huitle, L.S. Andrade, Electrocatalysis in wastewater treatment: recent mechanism advances, Quim. Nova, 34 (2011) 850–858.
[32] M. Bayramoglu, M. Kobya, O.T. Can, M. Sozbir, Operating cost analysis of electrocoagulation of textile dye wastewater, Sep. Purif. Technol., 37 (2004) 117–125.
[33] E. Butler, Y.-T. Hung, R.Y.-L. Yeh, M.S. Al Ahmad, Electrocoagulation in wastewater treatment, Water, 3 (2011) 495–525.
[34] H.W. Lin, C. Kustermans, E. Vaiopoulou, A. Prevoteau, K. Rabaey, Z. Yuan, I. Pikaar, Electrochemical oxidation of iron and alkalinity generation for efficient sulfide control in sewers, Water Res., 118 (2017) 114–120.
[35] C.E. Barrera-Díaz, V. Lugo-Lugo, B. Bilyeu, A review of chemical, electrochemical and biological methods for aqueous Cr(VI) reduction, J. Hazard. Mater., 223–224 (2012) 1–12.

[36] E. Węglarz-Tomczak, Ł. Górecki, Azo dyes – biological activity and synthetic strategy, Chemik, 66 (2012) 1298–1307.
[37] F. Ghanbari, M. Moradi, Electrooxidation Processes for Dye Degradation and Colored Wastewater Treatment, R.K. Gautam, M.C. Chattopadhayaya, Eds., Advanced Nanomaterials for Wastewater Remediation, 1st ed., CRC Press, London, 2016, pp. 61–108.
[38] A. Lopez, H. Benbelkacem, J.S. Pic, H. Debellefontaine, Oxidation pathways for ozonation of azo dyes in a semi-batch reactor: a kinetic parameters approach, Environ. Technol., 25 (2004) 311–321.
[39] Z. Mandić, B. Nigović, B. Šimunić, The mechanism and kinetics of the electrochemical cleavage of azo bond of 2-hydroxy-5-sulfophenyl-azo-benzoic acids, Electrochim. Acta, 49 (2004) 607–615.
[40] K.A. Matis, E.N. Peleka, Alternative flotation techniques for wastewater treatment: focus on electroflotation, Sep. Sci. Technol., 45 (2010) 2465–2474.
[41] I. de Oliveira da Mota, J.A. de Castro, R. de Góes Casqueira, A.G. de Oliveira Junior, Study of electroflotation method for treatment of wastewater from washing soil contaminated by heavy metals, J. Mater. Res. Technol., 4 (2015) 109–113.
[42] V.A. Kolesnikov, V.I. Il'in, A.V. Kolesnikov, Electroflotation in wastewater treatment from oil products, dyes, surfactants, ligands, and biological pollutants: a review, Theor. Found. Chem. Eng., 53 (2019) 251–273.
[43] T. Muddemann, D. Haupt, M. Sievers, U. Kunz, Electrochemical reactors for wastewater treatment, ChemBioEng Rev., 6 (2019) 142–156.
[44] M. Valica, S. Hostin, Electrochemical treatment of water contaminated with methylorange, Nova Biotechnol. Chim., 15 (2016) 55–64.
[45] V. López-Grimau, M. Riera-Torres, M. López-Mesas, C. Gutiérrez-Bouzán, Removal of aromatic amines and decolourisation of azo dye baths by electrochemical treatment, Color. Technol., 129 (2013) 267–273.
[46] R. Jain, N. Sharma, K. Radhapyari, Electrochemical treatment of pharmaceutical azo dye amaranth from wastewater, J. Appl. Electrochem., 39 (2009) 577–582.
[47] S. Palanisamy, P. Nachimuthu, M.K. Awasthi, B. Ravindran, S.W. Chang, M. Palanichamy, D.D. Nguyen, Application of electrochemical treatment for the removal of triazine dye using aluminium electrodes, J. Water Supply Res. Technol. AQUA, 69 (2020) 345–354.
[48] T. Droguett, J. Mora-Gómez, M. García-Gabaldón, E. Ortega, S. Mestre, G. Cifuentes, V. Pérez-Herranz, Electrochemical degradation of Reactive Black 5 using two-different reactor configuration, Sci. Rep., 10 (2020) 1–11.
[49] M. Sala, M.C. Gutiérrez-Bouzán, Electrochemical techniques in textile processes and wastewater treatment, Int. J. Photoenergy, 3–4 (2012) 1–12.
[50] K. Sathishkumar, M.S. AlSalhi, E. Sanganyado, S. Devanesan, A. Arulprakash, A. Rajasekar, Sequential electrochemical oxidation and bio-treatment of the azo dye Congo red and textile effluent, J. Photochem. Photobiol., B, 200 (2019) 1–7.
[51] S.S. Vaghela, A.D. Jethva, B.B. Mehta, S.P. Dave, S. Adimurthy, G. Ramachandraiah, Laboratory studies of electrochemical treatment of industrial azo dye effluent, Environ. Sci. Technol., 39 (2005) 2848–2855.
[52] C.N. Brito, M. Barbosa Ferreira, E.C.M. de Moura Santos, J.J. Línares Léon, S.O. Ganiyu, C.A. Martinez-Huitle, Electrochemical degradation of azo-dye Acid Violet 7 using BDD anode: effect of flow reactor configuration on cell hydrodynamics and dye removal efficiency, J. Appl. Electrochem., 48 (2018) 1321–1330.
[53] M. Łuba, T. Mikołajczyk, B. Pierożyński, L. Smoczyński, P. Wojtacha, M. Kuczyński, Electrochemical degradation of industrial dyes in wastewater through the dissolution of aluminum sacrificial anode of Cu/Al macro-corrosion galvanic cell, Molecules, 25 (2020) 1–17.
[54] D. Lakshmanan, D.A. Clifford, G. Samanta, Ferrous and ferric ion generation during iron electrocoagulation, Environ. Sci. Technol., 43 (2009) 3853–3859.
[55] K. Xiao, Z. Li, J. Song, Z. Bai, W. Xue, J. Wu, C. Dong, Effect of concentrations of $Fe^{2+}$ and $Fe^{3+}$ on the corrosion behavior of carbon steel in $Cl^-$ and $SO_4^{2-}$ aqueous environments, Met. Mater. Int., 27 (2021) 2623–2633.
[56] X. Li, L. Liu, Y. Wu, T. Liu, Determination of the redox potentials of solution and solid surface of Fe(II) associated with iron oxyhydroxides, ACS Earth Space Chem., 3 (2019) 711–717.
[57] K. Xiao, C.F. Dong, X.G. Li, F.M. Wang, Corrosion products and formation mechanism during initial stage of atmospheric corrosion of carbon steel, J. Iron. Steel Res. Int., 15 (2008) 42–48.
[58] J.R. Macdonald, Impedance Spectroscopy – Emphasizing Solid Materials and Systems, Wiley-Interscience, New York 1987.
[59] M. Ingelsson, N. Yasri, E.P.L. Roberts, Electrode passivation, faradaic efficiency, and performance enhancement strategies in electrocoagulation – a review, Water Res., 187 (2020) 1–25.
[60] A. Gadd, D. Ryan, J. Kavanagh, A.L. Beaurain, S. Luxem, G. Barton, Electrocoagulation of fermentation wastewater by low carbon steel (Fe) and 5005 aluminium (Al) electrodes, J. Appl. Electrochem., 40 (2010) 1511–1517.
[61] J. Vidal, C. Espinoza, N. Contreras, R. Salazar, Elimination of industrial textile dye by electrocoagulation using iron electrodes, J. Chil. Chem. Soc., 62 (2017) 3519–3524.
[62] H. Luo, H. Su, C. Dong, X. Li, Passivation and electrochemical behaviour of 316L stainless steel in chlorinated simulated concrete pore solution, Appl. Surf. Sci., 400 (2017) 38–48.
[63] R. Cabrera-Sierra, E. Sosa, M.T. Oropeza, I. Gonzalez, Electrochemical study on carbon steel corrosion process in alkaline sour media, Electrochim. Acta, 47 (2002) 2149–2158.
[64] M.M. El-Naggar, Cyclic voltammetric studies of carbon steel in deaerated $NaHCO_3$ solution, J. Appl. Electrochem., 34 (2004) 911–918.
[65] C. Nie, J. Dong, P. Sun, C. Yan, H. Wu, B. Wang, An efficient strategy for full mineralization of an azo dye in wastewater: a synergistic combination of solar thermo- and electrochemistry plus photocatalysis, RSC Adv., 7 (2017) 36246–36255.
[66] Z. Wang, L. Ai, Y. Huang, J. Zhang, S. Li, J. Chen, F. Yang, Degradation of azo dye with activated peroxygens: when zero-valent iron meets chloride, RSC Adv., 7 (2017) 30941–30948.
[67] Y.-N. Liu, X. Zhou, X. Wang, K. Liang, Z.-K. Yang, C.-C. Shen, M. Imran, S. Sahar, A.-W. Xu, Hydrogenation/oxidation induced efficient reversible color switching between methylene blue and leuco-methylene blue, RSC Adv., 7 (2017) 30080–30085.
[68] B. Krishnakumar, M. Swaminathan, Influence of operational parameters on photocatalytic degradation of genotoxic azo dye Acid Violet 7 in aqueous ZnO suspensions, Spectrochim. Acta, Part A, 81 (2011) 739–744.
[69] B.E. Conway, B. Pierozynski, A.c. impedance behaviour of processes involving adsorption and reactivity of guanidonium-type cations at Pt(1 0 0) surface, J. Electroanal. Chem., 622 (2008) 10–14.
[70] B. AitHaddou, D. Chebabe, A. Dermaj, H. Benassaoui, A. El Assyry, N. Hajjaji, S.I. Ahmed, A. Srihiri, Comparative study of low carbon steel corrosion inhibition in 1 M HCl by 1,2,4-triazole-5-thione derivatives, J. Mater. Environ. Sci., 7 (2016) 2191–2200.

**Supplementary information**

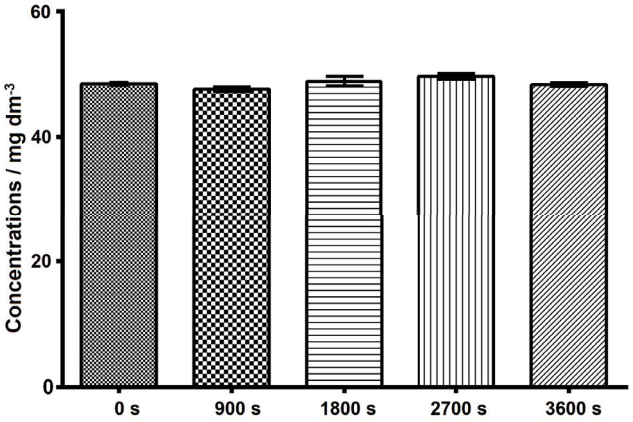


Fig. S1. Quantitative dye assay after only aeration (by slow purging of compressed oxygen to reach the value of *ca.* 10.5 ppm of dissolved oxygen) for the wavelength of 470 nm.

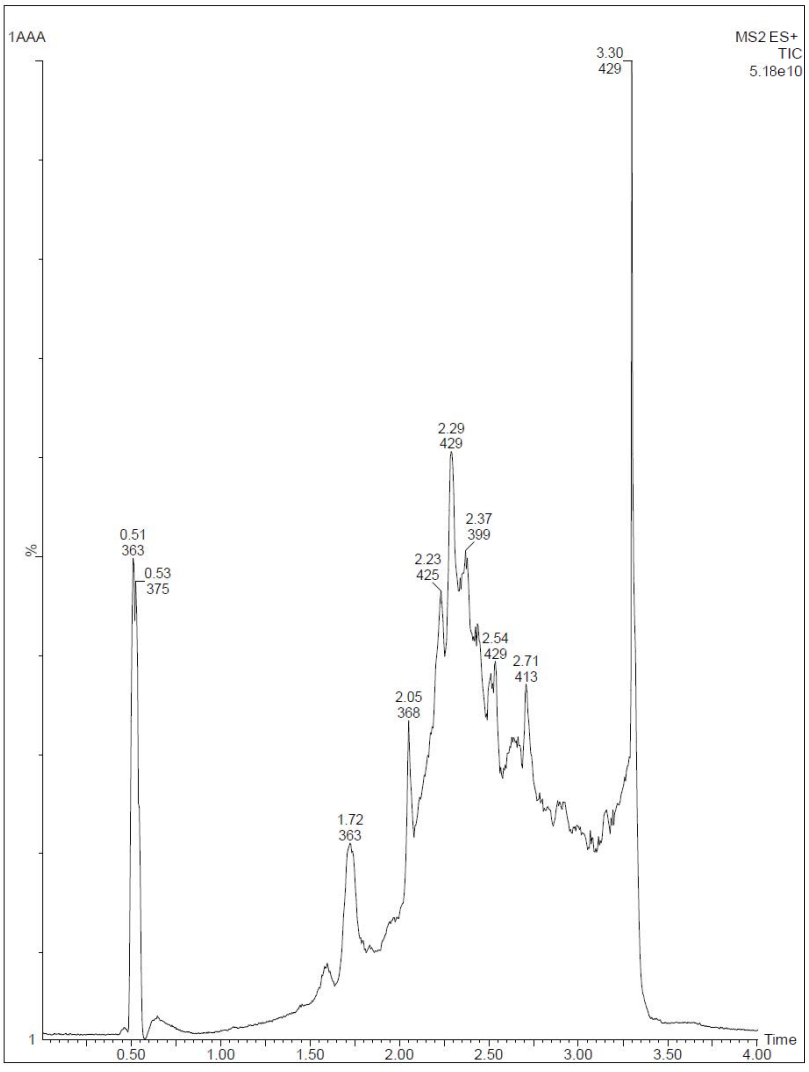


Fig. S2. Representative UPLC-MS/MS scan chromatogram for DR167 after the continuous voltammetric cycling (100 cycles, restricted to the potential range of the oxidation peak centered at –0.3 V).

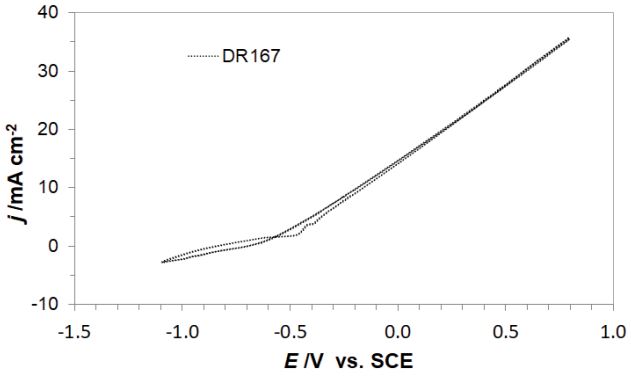


Fig. S3. Cyclic voltammetry for macro-corrosion Cu/Fe galvanic cell in the presence of DR167 dye in $Na_2SO_4$-based solution, recorded for the second CV sweep at a scan rate of 50 mV/s.

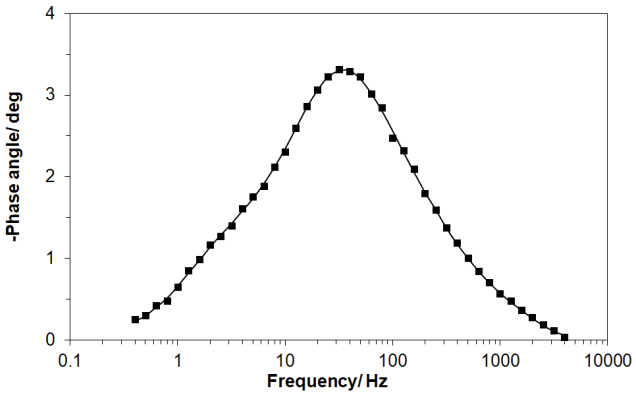


Fig. S4. Complex-plane bode impedance plot for Fe mild steel electrode in contact with DR167-modified (50 mg/dm$^3$) $Na_2SO_4$ solution derived for the potential of –330 mV vs. saturated calomel electrode (solid lines correspond to representation of the data according to an equivalent circuit model shown in Fig. 4)

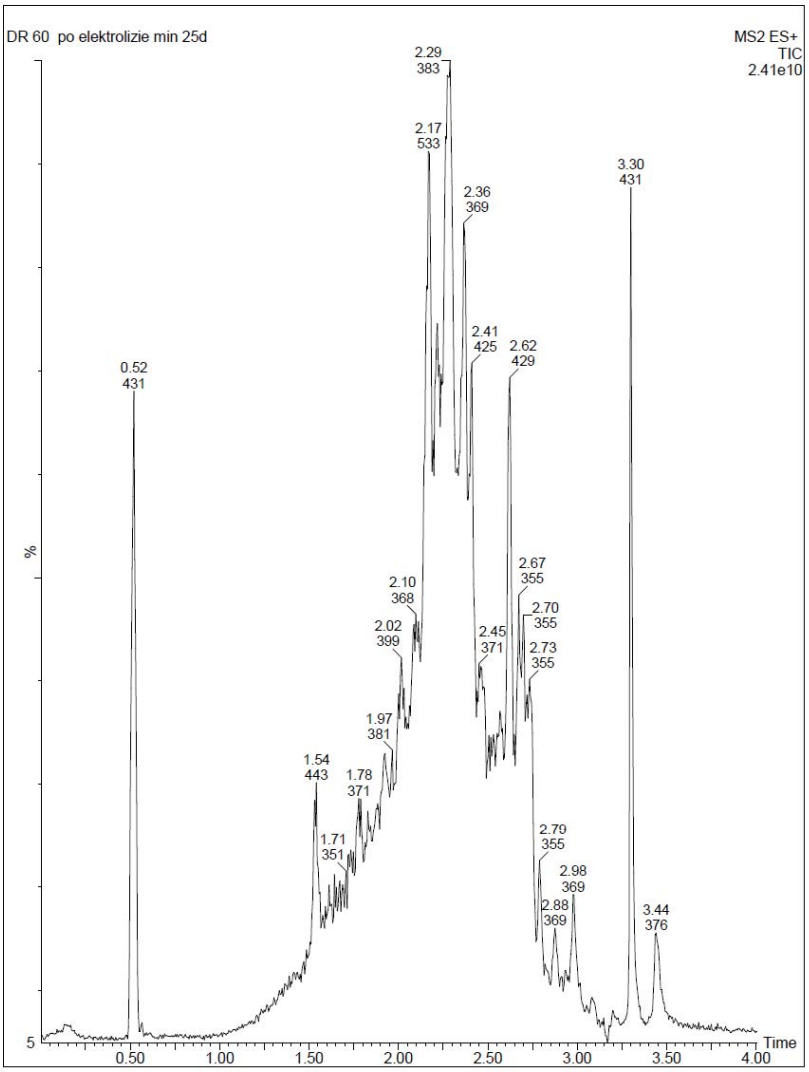


Fig. S5. Representative UPLC-MS/MS scan chromatogram for DR167 after 60 min of continuous electrolysis.